JOURNAL OF MATERIALS SCIENCE 11 (1976) 83–88

The effects of notch and fibre angles on crack propagation in fibre-reinforced polymers

B. SPENCER, J.T. BARNBY
Department of Metallurgy, University of Aston, Birmingham, UK

A critical stress intensity factor, related to an experimental crack length/compliance function, is used to specify the fracture resistance of a fibre-reinforced polymer. The effects of crack and/or fibre misorientation from the stress axis are experimentally measured and fitted to multiple regression equations containing variables shown experimentally to be significant. Resolution of the mode I and mode II contributions to fracture shows an extra contribution in the fibre composites as opposed to elastically isotropic and homogeneous materials.

1. Introduction

Fibre-reinforced materials are examples of elastically anistropic and inhomogeneous materials. We consider here only unidirectionally reinforced materials with continuous fibres. These are elastically orthotropic and inhomogeneous. In an earlier paper [1], attention was drawn to the fact that the dependence of the compliance of a cracked body on crack length, for this kind of material, is significantly different to that of an elastic continuum. Thus a K-calibration [2] curve must be determined experimentally. Further the use of a critical stress intensity factor as a criterion for fracture does not rest on the fact that K expresses the level of an $r^{-1/2}$ stress singularity at the crack tip as suggested by Sih *et al.* [3]. Indeed the stress singularity for the unidirectionally reinforced material with a crack extending at 90° to the fibre direction is better described as obeying a log $1/r$ than $1/\sqrt{r}$ law [4].

The theoretical result derived by Tirosh [4] allows for the anisotropy of the material and crack blunting effects. However, the anisotropy and the local elastic inhomogeneity effects may give rise to cross influences or coupling effects of elastic displacements [3] which could significantly affect the stored elastic strain energy which constitutes the driving force for fracture. Such effects are likely to be of more importance when the crack direction, or the fibre direction, or both are varied in relation to an applied tensile stress. Since the macro-mechanics and micromechanics of such a situation are extremely complex if all possible coupling effects are envisaged, the problem is approached here through statistical methods in order to discover the most significant coupling effects on simple parameters. Such an approach leads to a useable technology, and also may serve as a guide to the appropriate coupling factors which should be incorporated into a rigorous mechanics of the situation.

The approach; as in [1], is to use a quantity K, analogous to the stress intensity factor for isotropic materials, and then use its form as a definition for a K for the anistropic and elastically inhomogeneous material, this K being related to the actual strain energy content through an experimentally determined K-calibration curve. Taking this approach to the angled crack problem we note that for isotropic materials a number of authors [5–8] have found that the angled crack effectively concentrated the resolved normal and shear components, σ_N and τ of an applied stress σ. These components, as shown in Fig. 1, are:

$$\sigma_N = \sigma \sin^2 \theta \quad (1)$$

$$\tau = \sigma \sin \theta \cos \theta. \quad (2)$$

Thus the crack behaves as if it has a superposition of modes I and II such that for the

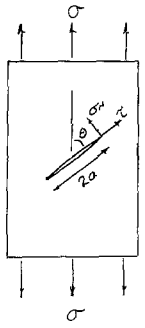

Figure 1 Model for the normal and shear stresses concentrated by the presence of a crack in a centre cracked plate.

Griffith geometry:

$$K_I = \sigma_N \sqrt{(\pi a)} \quad (3)$$

$$K_{II} = \tau \sqrt{(\pi a)}. \quad (4)$$

Defining the apparent stress intensity factor K_A as:

$$K_A = \sigma \sqrt{(\pi a)}, \quad (5)$$

then

$$K_I = K_A \sin^2 \theta \quad (6)$$

$$K_{II} = K_A \sin \theta \cos \theta. \quad (7)$$

The specific body geometry is now eliminated if we obtain K_A from the appropriate K calibration curve for any particular geometry by first using the crack length/gross width ratio along the line of the crack as in Fig. 2, then deriving K_I and K_{II}.

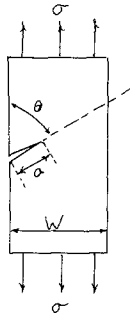

Figure 2 Model of the single edge notch tension specimens showing the notch angle θ, the crack length a, and the effective gross width W.

Crack extension in an isotropic material is then found to occur at a K_I and K_{II} combination which obeys the elliptical function:

$$\left(\frac{K_I}{K_{IC}}\right)^2 + \left(\frac{K_{II}}{K_{IIC}}\right)^2 = 1; \quad K_{IC} > K_{IIC}. \quad (8)$$

Here K_{IC} and K_{IIC} are the critical values for K_I and K_{II} when these modes are applied independently.

The fracture failure criterion above is consistent with a constant elastic strain energy content at crack extension as expressed by:

$$C_I K_I^2 = C_2 K_{II}^2 = G \text{ total}. \quad (9)$$

Here C_1 and C_2 are the appropriate compliance constants and G is the Irwin crack driving force. Experimental work on an orthotropic material has been shown to be in agreement with this criterion in some cases [9], although not in agreement with this criterion in other cases where failure obeyed [10].

$$\left(\frac{K_I}{K_{IC}}\right)^1 + \left(\frac{K_{II}}{K_{IIC}}\right)^2 = 1 \quad (10)$$

Generally, it is found that $K_{IIC} < K_{IC}$ [8] so that the super-position of a K_{II} component is of considerable significance.

In the work described below, the K-calibration curve for a crack extending normal to the fibre direction and for tensile stressing alone the fibres is intensionally used for K_A. This procedure relates the critical strain energy content when the crack and/or fibres are angled to the tensile stress, to the strain energy content when the crack is normal to, and the fibres parallel to the tensile axis. The objective is, therefore, to establish a practical way of allowing for angled cracks in terms of allowable defect sizes for given working stresses.

2. Experimental methods and materials

The material used was the same glass fibre/epoxide resin composite described in [1]. Specimens were also manufactured in the same way, as single edge

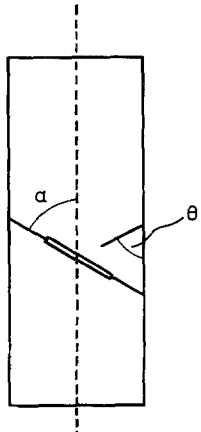

θ	a_1	a_2	a_3	a_4
90	0	45	45	90
75	15	30	60	70
65	25	20	70	65
55	35	10	80	55
45	45	0	90	45

Figure 3 Diagrams of the range of specimen types tested.

TABLE I Test results for combined modes I and II

Specimen No.	W (mm)	B (mm)	a (mm)	θ (deg)	α (deg)	K_A (MN m$^{-3/2}$)	K_{IA} (MN m$^{-3/2}$)	K_{IIA} (MN m$^{-3/2}$)
A1(i)	27.31	3.23	11.12	90	0	13.26	13.26	0
A1(ii)	28.42	3.28	12.44	90	0	14.36	14.36	0
A1(iii)	25.71	3.30	11.86	90	0	15.10	15.10	0
A2A(i)	27.90	3.35	13.72	90	45	5.35	5.35	0
A2A(ii)	25.61	3.38	12.29	90	45	4.25	4.25	0
A2A(iii)	28.31	3.37	13.73	90	45	3.94	3.94	0
A2B(i)	23.24	3.43	11.81	90	45	5.81	5.81	0
A2B(ii)	23.06	3.29	11.05	90	45	4.29	4.29	0
A2B(iii)	23.20	3.32	11.16	90	45	4.69	4.69	0
A3(i)	29.00	3.38	13.23	90	90	3.83	3.83	0
A3(ii)	28.91	3.35	14.06	90	90	3.37	3.37	0
A3(iii)	29.26	3.43	14.44	90	90	3.54	3.54	0
B1(i)	27.25	3.10	13.77	75	15	9.03	8.42	2.26
B1(ii)	26.92	3.15	13.63	75	15	5.02	4.69	1.26
B1(iii)	29.27	3.12	14.77	75	15	10.85	10.12	2.71
B2A(i)	26.22	3.33	13.54	75	30	9.22	8.60	2.30
B2A(ii)	27.66	3.25	13.41	75	30	11.28	10.52	2.82
B2A(iii)	28.37	3.20	13.06	75	30	8.68	8.10	2.17
B2B(i)	28.48	3.35	14.58	75	60	5.80	5.41	1.45
B2B(ii)	26.56	3.35	15.00	75	60	6.97	6.50	1.74
B2B(iii)	28.00	3.35	12.65	75	60	4.59	4.28	1.15
B3(i)	27.65	3.40	13.69	75	75	4.45	4.16	1.11
B3(ii)	28.60	3.42	13.94	75	75	4.02	3.75	1.00
B3(iii)	29.10	3.41	14.12	75	75	4.49	4.19	1.12
C1(i)	29.46	3.28	14.24	65	25	11.64	9.56	4.46
C1(ii)	29.08	3.40	14.92	65	25	10.49	8.62	4.02
C1(iii)	34.30	3.15	17.16	65	25	5.80	4.77	2.22
C2A(i)	26.87	3.51	14.40	65	20	12.84	10.55	4.92
C2A(ii)	26.33	3.48	14.89	65	20	12.83	10.54	4.92
C2A(iii)	28.12	3.45	14.89	65	20	13.88	11.40	5.32
C2B(i)	27.86	3.18	14.89	65	70	5.39	4.43	2.06
C2B(ii)	27.35	3.20	14.96	65	70	5.60	4.60	2.15
C2B(iii)	27.76	3.20	14.80	65	70	3.84	3.15	1.47
C3(i)	27.44	3.28	14.86	65	65	6.68	5.49	2.56
C3(ii)	27.18	3.30	13.68	65	65	5.27	4.33	2.02
C3(iii)	31.09	3.23	14.80	65	65	8.42	6.92	3.23
D1(i)	28.35	3.44	14.57	55	35	11.05	7.41	5.19
D1(ii)	29.91	3.20	14.50	55	35	7.95	5.34	3.74
D1(iii)	29.05	3.18	14.25	55	35	7.70	5.17	3.62
D2A(i)	24.19	3.61	13.69	55	10	26.37	17.70	12.39
D2A(ii)	25.59	3.60	13.15	55	10	18.36	12.32	8.63
D2A(iii)	24.64	3.55	12.65	55	10	20.64	13.85	9.70
D2B(i)	25.69	3.47	13.73	55	80	4.66	3.13	2.19
D2B(ii)	29.23	3.50	13.28	55	80	6.48	4.35	3.04
D2B(iii)	29.81	3.30	14.10	55	80	5.60	3.76	2.63
D3(i)	24.07	3.28	13.26	55	55	7.02	4.71	3.30
D3(ii)	24.42	3.33	13.17	55	55	7.48	5.02	3.51
D3(iii)	26.40	3.28	12.87	55	55	6.65	4.46	3.12

Table I continued

TABLE I Test results for combined modes I and II – *continued*

Specimen No.	W (mm)	B (mm)	a (mm)	θ (deg)	α (deg)	K_A (MN m$^{-3/2}$)	K_{IA} (MN m$^{-3/2}$)	K_{IIA} (MN m$^{-3/2}$)
E1(i)	25.17	3.29	11.66	45	45	11.51	5.75	5.75
E1(ii)	21.15	3.41	9.99	45	45	9.74	4.87	4.87
E1(iii)	20.82	3.34	13.99	45	45	10.55	5.27	5.27
E2A(i)	25.29	3.47	13.53	45	0	33.87	16.94	16.94
E2A(ii)	26.40	3.49	13.22	45	0	28.72	14.36	14.36
E2A(iii)	25.81	3.49	14.45	45	0	37.40	18.70	18.70
E2B(i)	26.83	3.27	16.08	45	90	8.82	4.41	4.41
E2B(ii)	24.53	3.29	15.60	45	90	5.55	2.77	2.77
E2B(iii)	25.31	3.27	14.68	45	90	10.95	5.47	5.47
E3(i)	22.90	3.34	13.07	45	45	10.14	5.07	5.07
E3(ii)	22.94	3.40	10.73	45	45	9.02	4.51	4.51
E3(iii)	28.42	3.30	13.90	45	45	7.33	3.66	3.66

notched tension pieces, cut with a diamond saw from 3.1 mm thick sheet. The angle, α, between the fibre axis and the tension axis was varied by cutting samples from the sheet at various angles. Notches were cut at various angles θ to the loading axis. The range of specimens tested is illustrated in Fig. 3. Notches were sharpened again by extending the 2 mm wide slots 1.5 mm using a 0.25 mm thick jewellers' saw. The K-calibration curve used was that for fibres at $\alpha = 0$ and the notch at $\theta = 90°$ as described in [1].

Mechanical testing was carried out on an Instron machine at a cross-head speed of 0.2 mm min^{-1}. A clip gauge was mounted on the edge of the specimen and gave an electrical signal linearly related to the opening displacement at the mouth of the notch.

3. Results

Load versus crack opening displacement traces were linear up to the onset of failure for all except the cases where $\alpha = 0, \theta = 90°$. Typical traces showing load versus displacement are shown in Fig. 4. The fracture load is unambiguously the maximum load on the trace. Tests for each combination of α and θ were carried out in triplicate. The values of a/w were measured as shown in Fig. 2, and the apparent K, namely K_A, determined using the K-calibration curve as reported in [1]. The K_{IA} and K_{IIA} were derived as $K_A \sin^2\theta$ and $K_A \sin\theta \cos\theta$ respectively. The experimental results are shown in Table I. An initial statistical analysis was carried out to determine whether K_A, K_{IA} and K_{IIA}, independently were significantly dependent on α, θ and $\alpha\theta$. The tests showed significant dependences in all cases.

In view of this preliminary result multiple regression analyses were carried out on K_A, K_{IA} and K_{IIA} respectively. The chosen variables were θ, α, $\sin\theta$, $\cos\theta$, $\sin\alpha$, $\cos\alpha$ and $\alpha\theta$. All variables shown not to be significant at the 5% level were eliminated and the multiple regression performed again to obtain the coefficients of the significant terms. Multiple correlation coefficients were then derived for the regressions on the significant variables. The regression equations obtained were:

$$K_A = 44.51 - 0.35\,\theta - 36.14 \sin\alpha + 0.004\,\alpha\theta \quad (11)$$

(multiple correlation coefficient 0.919)

$$K_{IA} = 29.97 - 0.19\,\theta - 25.26 \sin\alpha + 0.002\,\alpha\theta \quad (12)$$

(multiple correlation coefficient 0.917)

$$K_{IIA} = 43.68 - 0.31\,\theta - 0.44\,\alpha - 14.65 \cos\alpha + 0.003\,\alpha\theta \quad (13)$$

(multiple correlation coefficient 0.947).

These equations were selected as having the highest correlation coefficients of the many trials. Deviation of the experimentally determined K_A values from those determined by the regression equation are shown graphically in Fig. 5. The variation of K_A with the misorientation of fibres from the loading axis shown in Fig. 6, as derived from the regression equation. Five notch angles are represented though any intermediate notch angle could, naturally, be plotted.

The multiple regression analysis of the K_{IA} showed that the effect of notch angle θ and of fibre angle, α, were highly significant. The regression for K_{IIA} again indicates a residual dependence on θ over and above that assumed in "resolving" from K_A.

TABLE II Values of Young's modulus versus fibre orientation

Fibre orientation to loading axis (Deg)	Young's modulus ($MN\,m^{-2} \times 10^4$)
0	4.72
10	4.57
15	3.98
20	3.43
25	3.20
30	2.48
35	2.10
45	1.89
55	1.61
60	1.60
65	1.57
70	1.46
75	1.55
80	1.54
90	1.79

In addition to measurements of the toughness of notched samples, the Young's modulus in the direction of the tensile axis was measured, as in [1], for unnotched coupons. The results showing the variation of Young's modulus, as the fibre direction was rotated in relation to the tensile axis, are shown in Table II.

4. Discussion

Table I shows that individual toughnesses at a given combination of α and θ may be measured quite accurately and reproducibly. Thus the basic data for the regression analyses are good. Further the fracture load is quite unambiguous as shown by Fig. 4. Naturally the structure of the fibre-reinforced composite is somewhat irregular on a microscale, and this combined with a less than perfect regression on the significant variables contributes to the scatter shown graphically in Fig. 5. Nevertheless the results in all cases give multiple regression coefficients of greater than 0.9. Consequently, plots such as Fig. 6 allow K_A to be determined with 95% confidence, for any α or θ combination. This is normally a sound basis for technological application. The application of the method, therefore, allows maximum working stresses to be determined for given defect sizes, or vice versa. Of course safety factors would be introduced appropriate to a practical application.

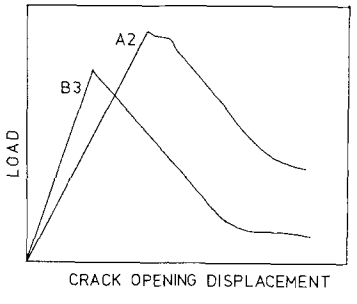

Figure 4 Examples of load/crack opening displacement traces for specimens A2 ($\theta = 90°$, $\alpha = 45°$) and B3 ($\theta = 75°$, $\alpha = 75°$).

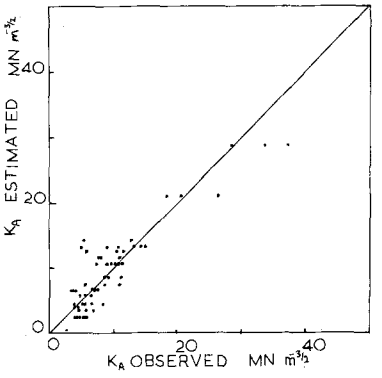

Figure 5 Plot of experimentally measured K_A at fracture against the estimated K_A using the regression equation.

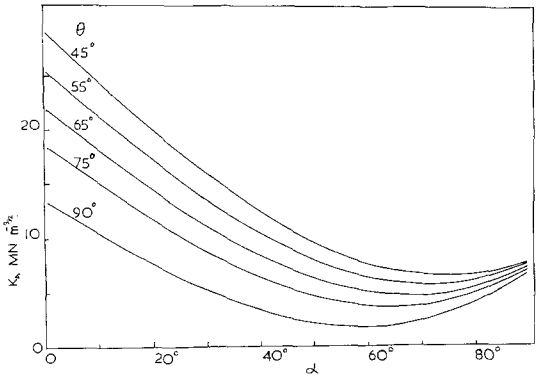

Figure 6 Plot of K_A versus α for $\theta = 45°$, 55°, 65°, 75° and 90° using the regression equation.

The plots of Fig. 6 all indicate minimum around $\alpha \simeq 70°$. Recalling that the data are related to the compliance function for $\theta = 90°$ and $\alpha = 0°$ it is probable that the minimum arises partly because of the extra stored elastic strain energy at a given load for the less stiff fibre orientations. Indeed we find this is consistent with the minimum in Young's Modulus shown in Table II which also occurs at about $\alpha = 70°$.

In the definition of K_{IA} is incorporated the assumption that the main dependence of K_A on θ arises from the fact that only the component of direct stress normal to the notch faces is concentrated by the presence of the defect. Therefore, the contribution to the opening mode of fracture is fully allowed for by taking $K_A \sin^2\theta$. This is confirmed by experiment [6] on isotropic materials

but the results do not confirm this interpretation for the inhomogeneous orthotropic material since there is a significant residual dependence of K_{IA} on θ.

Experiments [6] on isotropic materials similarly confirm that the K_{II} contribution for the angled crack problem arises simply from the defect concentrating the resolved shear stress along its surface. In our case this would result in no dependence of K_{IIA} on θ. However, we find there is, in fact, a residual dependence of K_{IIA} on θ. This is likely to arise from extra shear stresses, in the vicinity of the defect, transmitted by the fibres.

The highly significant regression equations express the effects of fibre angle and notch angle in terms of quite simple and separate functions of α and θ, with the exception of the product $\alpha\theta$. The presence of this term certainly affects the significance levels of the regressions. It is, therefore, not surprising that in the failure criterion:

$$\left(\frac{K_I}{K_{IC}}\right)^m + \left(\frac{K_{II}}{K_{IIC}}\right)^n = 1 \qquad (14)$$

results for orthotropic material [10] have been found to support $m = 1$ and $n = 2$ in contrast to the results expected for isotropic materials, $m = n = 2$. However, a full test of this criterion is beyond the scope of the experimental work presented here.

References

1. J. T. BARNBY and B. SPENCER, *J. Mater. Sci.* 11 (1976) 78.
2. W. F. BROWN and J. E. SRAWLEY, A.S.T.M., S.T.P. 410 (1967).
3. G. C. SIH, P. C. PARIS and G. R. IRWIN, *Int. J. Fract. Mech.* 1 (1965) 189.
4. J. TIROSH, *J. Appl. Mechs.* 40 (1973) 785.
5. W. K. WILSON, W. G. CLARK and E. T. WESSEL, Westinghouse Research Labs. Rpt. No. 10276 (1968).
6. L. P. POOK, National Eng. Labs. Rpt. 449 (1970).
7. B. C. HOSKIN, D. G. GRAFF and P. J. FODEN, A.R.L. 8M 305, Melbourne (1965).
8. H. LIEBOWITZ, "Fracture Mechanics of Aircraft Structures", AGARDograph No. 176 (1974) p. 145.
9. R. J. SANDFORD and S. R. STONESIFER, Naval Research Lab. Rpt. 7112 (1970).
10. E. M. WU, *Trans. ASME* E34 (1967) 967.

Received 28 April and accepted 26 June 1975.